

# 1 **Insights into Soil NO Emissions and the Contribution to Surface** 2 **Ozone Formation in China**

3  
4 Ling Huang<sup>1,2</sup>, Jiong Fang<sup>1,2</sup>, Jiaqiang Liao<sup>1,2</sup>, Greg Yarwood<sup>3</sup>, Hui Chen<sup>1,2</sup>, Yangjun Wang<sup>1,2</sup>, Li Li<sup>1,2\*</sup>

5  
6 <sup>1</sup>School of Environmental and Chemical Engineering, Shanghai University, Shanghai, 200444, China

7 <sup>2</sup>Key Laboratory of Organic Compound Pollution Control Engineering (MOE), Shanghai University,  
8 Shanghai, 200444, China

9 <sup>3</sup>Ramboll, Novato, California, 94945, USA

10  
11 Correspondence: Li Li (lily@shu.edu.cn)

12  
13 **Keywords:** Soil NO emissions; Ground-level ozone; BDSNP; OSAT

14  
15 **Abstract.** Elevated ground-level ozone concentrations have emerged as a major  
16 environmental issue in China. Nitrogen oxide (NO<sub>x</sub>) is a key precursor to ozone formation.  
17 Although control strategies aimed at reducing NO<sub>x</sub> emissions from conventional combustion  
18 sources are widely recognized, soil NO<sub>x</sub> emissions (mainly as NO) due to microbial processes  
19 have received little attention. The impact of soil NO emissions on ground-level ozone  
20 concentration is yet to be evaluated. This study estimated soil NO emissions in China using  
21 the Berkeley-Dalhousie soil NO<sub>x</sub> parameterization (BDSNP) algorithm. A typical modeling  
22 approach was used to quantify the contribution of soil NO emissions to surface ozone  
23 concentration. The Brute-force method (BFM) and the Ozone Source Apportionment  
24 Technology (OSAT) implemented in the Comprehensive Air Quality Model with extensions  
25 (CAMx) were used. The total soil NO emissions in China for 2018 were estimated to be  
26 1157.9 Gg N, with an uncertainty range of 715.7~1902.6 Gg N. Spatially, soil NO emissions  
27 are mainly concentrated in Central China, North China, Northeast China, northern Yangtze  
28 River Delta (YRD) and eastern Sichuan Basin, with distinct diurnal and monthly variations  
29 that are mainly affected by temperature and the timing of fertilizer application. Both the BFM  
30 and OSAT results indicate a substantial contribution of soil NO emissions to the maximum  
31 daily 8-hour (MDA8) ozone concentrations by 8~12.5 μg/m<sup>3</sup> on average for June 2018, with  
32 the OSAT results consistently higher than BFM. The results also showed that soil NO  
33 emissions led to a relative increase in ozone exceedance days by 10%~43.5% for selected  
34 regions. Reducing soil NO emissions resulted in a general decrease in monthly MDA8 ozone  
35 concentrations, and the magnitude of ozone reduction became more pronounced with  
36 increasing reductions. However, even with complete reductions in soil NO emissions,  
37 approximately 450.3 million people are still exposed to unhealthy ozone levels, necessitating

38 multiple control policies at the same time. This study highlights the importance of soil NO  
39 emissions for ground-level ozone concentrations and the potential of reducing NO emissions  
40 as a future control strategy for ozone mitigation in China.

## 41 **1. Introduction**

42 A substantial decrease in the atmospheric fine particulate matter (PM<sub>2.5</sub>) concentrations has  
43 been witnessed during the past decade in China (Zhai et al., 2019; Xiao et al., 2020; Maji,  
44 2020) while the ground-level ozone (O<sub>3</sub>) concentrations do not exhibit a steady downward  
45 trend (Lu et al., 2020; Lu et al., 2021; Wang et al., 2022a; Sun et al., 2021). Because high  
46 ozone concentration increases respiratory and circulatory risks (Malley et al., 2017; Cakaj et  
47 al., 2023; Wang et al., 2020) and reduces crop yields (Feng et al., 2019; Lin et al., 2018;  
48 Mukherjee et al., 2021; Montes et al., 2022), the coordinate control of PM<sub>2.5</sub> and O<sub>3</sub> was  
49 proposed as part of the 14<sup>th</sup> Five-year plan (Council, 2021). A continuous increase in  
50 summertime surface ozone was observed across China's nationwide monitoring network from  
51 2013 to 2019, followed by an unprecedented decline in 2020 (except for Sichuan Basin) (Sun  
52 et al., 2021), which is equally attributed to meteorology and anthropogenic emissions  
53 reductions (Yin et al., 2021). As a secondary air pollutant, ozone is generated by the  
54 photochemical oxidation of volatile organic compounds (VOC) in the presence of nitrogen  
55 oxides (NO<sub>x</sub> = NO + NO<sub>2</sub>), both of which are considered ozone precursors. **The non-linear  
56 response of ozone formation to its precursors is well established (Kleinman et al., 1994;  
57 Sillman et al., 1990). In regions classified as NO<sub>x</sub>-limited, reducing NO<sub>x</sub> emissions is an  
58 effective strategy for ozone mitigation. However, in regions classified as VOC-limited,  
59 typically characterized by high NO<sub>x</sub> emissions such as metropolitan areas, decreasing NO<sub>x</sub>  
60 emissions may actually result in increased ozone concentrations due to reduced ozone titration  
61 by NO and diminished OH titration by NO<sub>2</sub> (Seinfeld and Pandis, 2016). Under such  
62 circumstances, reducing VOC emissions will counteract ozone increases caused by reducing  
63 NO<sub>x</sub> emissions.** The control strategies to mitigate ozone pollution in China focused on  
64 reducing NO<sub>x</sub> emissions at an early stage and started to stress the control of VOCs emissions  
65 in recent years (e.g., the 2020 action plan on VOCs mitigation), including control of fugitive  
66 emissions, stringent emissions standards, and substituting raw materials with low VOCs  
67 content (Ecology, 2020). Ding et al. (2021) concluded that for North China Plain (NCP), a  
68 region that experienced the most severe PM<sub>2.5</sub> and ozone pollution in China, reductions in  
69 NO<sub>x</sub> emissions are essential regardless of VOC reduction.

70 Existing control strategies for NO<sub>x</sub> emissions are almost exclusively targeted at combustion  
71 sources, for example, power plants, industrial boilers, cement production, and vehicle  
72 exhausts (Sun et al., 2018; Ding et al., 2017; Diao et al., 2018). However, NO<sub>x</sub> emissions from  
73 soils (mainly as NO), as a result of microbial processes (e.g., nitrification and denitrification),

74 could make up a substantial fraction of the total NO<sub>x</sub> emissions (Lu et al., 2021; Drury et al.,  
75 2021), yet is often overlooked. In California, soil NO<sub>x</sub> emissions in July accounted for 40% of  
76 the state's total NO<sub>x</sub> emissions (when using an updated estimation algorithm) and resulted in  
77 23% of enhanced surface ozone concentration (Sha et al., 2021). However, a wide range of  
78 annual soil NO<sub>x</sub> emissions from 8,685 tons (as NO<sub>2</sub>, (Guo et al., 2020) to 161,100 metric tons  
79 of NO<sub>x</sub>-N (Almaraz et al., 2018) were reported depending on different methods. Romer et al.  
80 (2018) estimated that nearly half of the increase in hot-day ozone concentration in a forested  
81 area of the rural southeastern United States is attributable to the temperature-induced  
82 increases in NO<sub>x</sub> emissions, mostly likely due to soil microbes.

83 Soil NO emissions are affected by many factors, including nitrogen fertilizer application, soil  
84 organic carbon content, soil temperature, humidity, and pH (Vinken et al., 2014; Yan et al.,  
85 2005; Wang et al., 2021; Skiba et al., 2021). The amount of nitrogen fertilizer application in  
86 China was estimated to account for one-third of the global nitrogen fertilizer application  
87 (Heffer and Prud'homme, 2016), with most of the land under high nitrogen deposition (Liu et  
88 al., 2013; Lü and Tian, 2007). Therefore, soil NO emissions in China are expected to be  
89 significant, and their impacts on ozone pollution need to be systematically evaluated. So far,  
90 only a limited number of studies have addressed this issue in China (Lu et al., 2021; Shen et  
91 al., 2023; Wang et al., 2008; Wang et al., 2022b). Lu et al. (2021) concluded that soil NO  
92 significantly reduced the ozone sensitivity to anthropogenic emissions in NCP, therefore,  
93 causing a so-called "emissions control penalty". Wang et al. (2022b) reported NO<sub>x</sub> emissions  
94 from cropland contributed 5.0% of the maximum daily 8h average ozone (MDA8 O<sub>3</sub>) and  
95 27.7% of NO<sub>2</sub> concentration in NCP. These studies focused solely on NCP, a region with  
96 persistent O<sub>3</sub> pollution in warm seasons (Liu et al., 2020; Lu et al., 2020). The impact of soil  
97 NO emissions on ozone concentrations over other regions, for example, the northern Yangtze  
98 River Delta (YRD) and Sichuan Basin, where soil emissions are high (see Section 3.1) and  
99 ozone pollution is also severe (Shen et al., 2022; Yang et al., 2021), has not been much  
100 evaluated in details (Shen et al., 2023). In addition, the method employed in existing studies  
101 to evaluate soil NO emissions on ozone concentration is the conventional "brute-force" zero-  
102 out approach, which might be inappropriate given the strong nonlinearity of the ozone  
103 chemistry (Clappier et al., 2017; Thunis et al., 2019).

104 With the deepening of emissions control measures for power, industrial and on-road sectors,  
105 anthropogenic NO<sub>x</sub> emissions from combustion sources have decreased at a much faster rate  
106 (by 4.9% since 2012) than that from soil (fertilizer application decreases at a rate of 1.5%  
107 since 2015, Fig. S1). Therefore, understanding the impacts of soil NO emissions on ground-  
108 level ozone concentration, particularly considering the spatial heterogeneities over different  
109 regions of China, is of great importance for formulating future ozone mitigation strategies. In  
110 this study, soil NO emissions in China for 2018 were estimated based on a most recent soil

111 NO parameterization scheme with updated fertilizer data as input. The spatial and temporal  
 112 variations of soil NO emissions were described first. Uncertainties associated with estimation  
 113 of soil NO emissions were discussed. An integrated meteorology and air quality model was  
 114 applied to quantify the impact of soil NO emissions on surface ozone concentration based on  
 115 two different methods. Lastly, we evaluated the changes in ozone concentration and exposed  
 116 population under different emission scenarios to highlight the effectiveness of reducing soil  
 117 NO emissions as potential control policy. Our results provide insights into developing  
 118 effective emissions reduction strategies to mitigate the ozone pollution in China.

## 119 **2. Methodology**

### 120 2.1. Estimation of soil NO emissions in China

121 Soil NO emissions were estimated based on the Berkeley-Dalhousie Soil NO<sub>x</sub>  
 122 Parameterization (BDSNP) that is implemented in the Model of Emissions of Gases and  
 123 Aerosols from Nature (MEGAN) version 3.2 (<https://bai.ess.uci.edu/megan/data-and-code>,  
 124 accessed on September 1<sup>st</sup>, 2021). The BDSNP algorithm estimates the soil NO emissions by  
 125 adjusting a biome-specific NO emissions factor in response to various conditions, including  
 126 the soil temperature, soil moisture, precipitation-induced pulsing, and a canopy reduction  
 127 factor (Eq. 1, (Rasool et al., 2016):

$$128 \text{ NO}_{\text{emission flux}} = A'_{\text{biome}}(N_{\text{avail}}) \times f(T) \times g(\theta) \times P(l_{\text{dry}}) \times \text{CRF}(\text{LAI}, \text{Biome}, \text{Meterology}) \quad \text{Eq. 1}$$

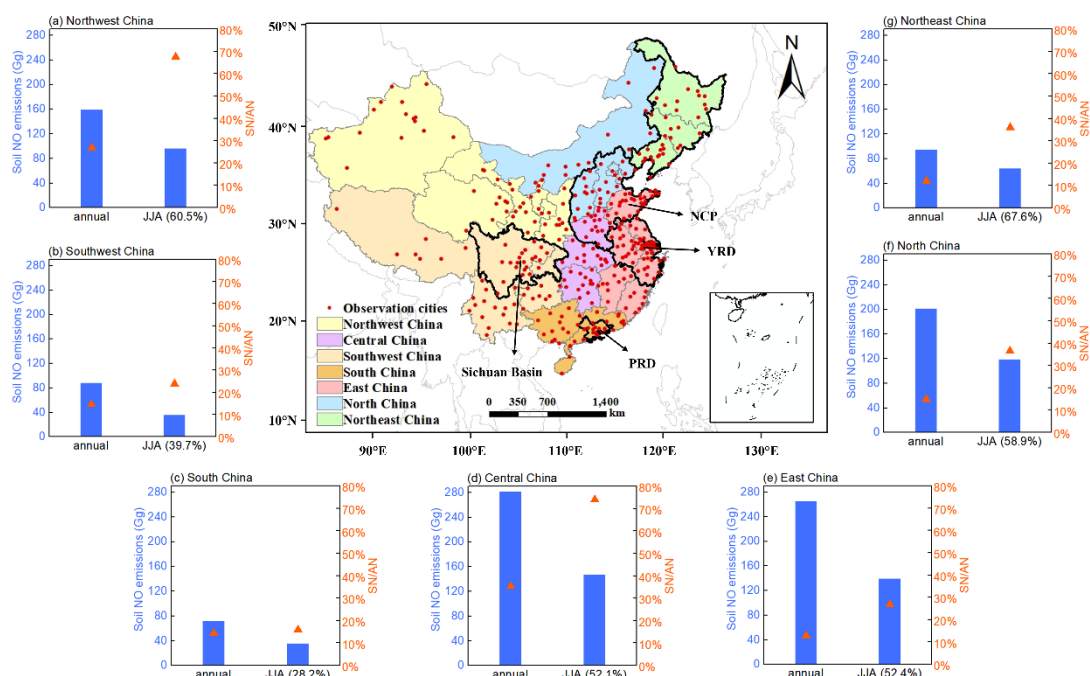
128 where  $f(T)$  and  $g(\theta)$  is the temperature ( $T$ , unit: K) and soil moisture ( $\theta$ , unit: m<sup>3</sup>/m<sup>3</sup>)  
 129 dependence functions, respectively;  $P(l_{\text{dry}})$  represents the pulsed soil emissions due to wetting  
 130 of dry soils;  $l_{\text{dry}}$  (hours) is the antecedent dry period of a pulse; and CRF describes the canopy  
 131 reduction factor, which is a function of the leaf area index (LAI, m<sup>2</sup>/m<sup>2</sup>) and the meteorology.  
 132  $A'_{\text{biome}}$  (ng N m<sup>-2</sup> s<sup>-1</sup>) is the biome-specific emission factor, which is further calculated as Eq.2:

$$A'_{\text{biome}} = A_{w,\text{biome}} + N_{\text{avail}} \times \bar{E} \quad \text{Eq. 2}$$

133 In Eq. 2,  $A_{w,\text{biome}}$  (ng N m<sup>-2</sup> s<sup>-1</sup>) is the wet biome-dependent emission factor;  $N_{\text{avail}}$  is the  
 134 available nitrogen from fertilizer and deposition;  $\bar{E}$  is the emission rate based on an observed  
 135 global estimates of fertilizer emissions ((Rasool et al., 2016). The detailed expressions of  
 136 these parameters are presented in the Supporting Information. More information on the  
 137 BDSNP parameterizations can be found in previous studies (Hudman et al., 2012).

138 The default N fertilizer input data provided with the BDSNP algorithm is based on the a  
 139 (Potter et al., 2010), which gives a number of 19.6 Tg N/a. In this study, we collected fertilizer  
 140 data from statistical yearbooks at the provincial level. The total amount of pure nitrogen  
 141 fertilizer (hereafter N fertilizer) applied in the year 2018 is 20.7 Tg N/a, which is similar  
 142 (5.6% higher) to IFA value. However, besides the N fertilizer, NPK compound fertilizer

143 (containing nitrogen (N), phosphorous (P), and potassium (K)) is being increasingly applied  
 144 in China. According to the statistical yearbook, the amount of N fertilizer applied decreased  
 145 from 23.5 Tg in 2010 to 20.7 Tg in 2018 (a relative reduction of 11.9%). In contrast, NPK  
 146 fertilizer increased from 18.0 in 2010 to 22.7 Tg in 2018 (a relative increase of 26.1%). We  
 147 assumed one-third of the NPK fertilizer is nitrogen (Liu, 2016); thus, the total amount of  
 148 nitrogen applied as fertilizer is 28.2 Tg N in 2018, which is 43.9% higher than the value from  
 149 Potter et al. (2010). We divided China into seven regions for emission analysis at regional  
 150 scale, namely Northeast China, North China, Central China, East China, South China,  
 151 Southwest China, and Northwest China, as indicated by different colors in Fig. 1 (see Table  
 152 S1 for the list of provinces in each region). At the regional level, the amount of total fertilizer  
 153 differs by as much as 9.1% to 46.4% from the default fertilizer (Table S2).



154  
 155 **Figure 1.** Modeling domain and region definitions. Surrounding charts show the annual and  
 156 summer (June-July-August, JJA) soil NO emissions and ratio of soil NO to anthropogenic  
 157 NO<sub>x</sub> emissions for each region.

158 **2.2. Model configurations**

159 A typical modeling approach was applied to evaluate the contribution of soil NO emissions to  
 160 surface ozone concentration. The Weather Research and Forecasting (WRF) model (version  
 161 3.7, <https://www.mmm.ucar.edu/wrf-model-general>, accessed on December 1<sup>st</sup>, 2021) and the  
 162 Comprehensive Air Quality Model with Extension (CAMx, version 7.0, <http://www.camx.com/>,  
 163 accessed on December 1<sup>st</sup>, 2021) were applied to simulate the  
 164 meteorological fields and subsequent ozone concentrations. Table S3 listed the detailed model  
 165 configurations for WRF and CAMx. Anthropogenic emissions include the Multi-resolution

166 Emission Inventory of China for 2017 (MEIC, <http://www.meicmodel.org>, accessed on  
167 December 1st, 2021) and the 2010 European Commission's Emissions Database for Global  
168 Atmospheric Research (EDGAR, <http://edgar.jrc.ec.europa.eu/index.php>, accessed on  
169 December 1st, 2021) for outside China. Biogenic emissions were calculated along with the  
170 soil NO emissions using MEGAN3.2. Open biomass burning emissions are adopted from the  
171 Fire INventory from NCAR version (FINN, version 1.5,  
172 <https://www.acom.ucar.edu/Data/fire/>) with MOZART speciation and converted to CAMx  
173 CB05 model species. The gaseous and aerosol modules used in CAMx include the CB05  
174 chemical mechanism (Yarwood et al., 2010) and the CF module. The aqueous-phase  
175 chemistry is based on the updated mechanism of the Regional Acid Deposition Model  
176 (RADM) (Chang et al., 1987). A base case simulation was conducted for June 2018 when soil  
177 NO emissions reached maxima (Section 3.1) and ozone pollution was severe over eastern  
178 China (Mao et al., 2020; Jiang et al., 2022). Base case model performances have been  
179 evaluated in our previous studies (Huang et al., 2021; Huang et al., 2022b). Here we evaluated  
180 simulated ozone concentrations using the Pearson correlation coefficient (R), mean bias  
181 (MB), root-mean-square error (RMSE), normalized mean bias (NMB), and normalized mean  
182 error (NME) against hourly observed ozone concentrations for 365 cities in China. The  
183 formula for each of the statistical metrics is given in Table S4. Observed hourly ozone  
184 concentrations were obtained from the China National Environmental Monitoring Center.

### 185 2.3. Brute-force and OSAT

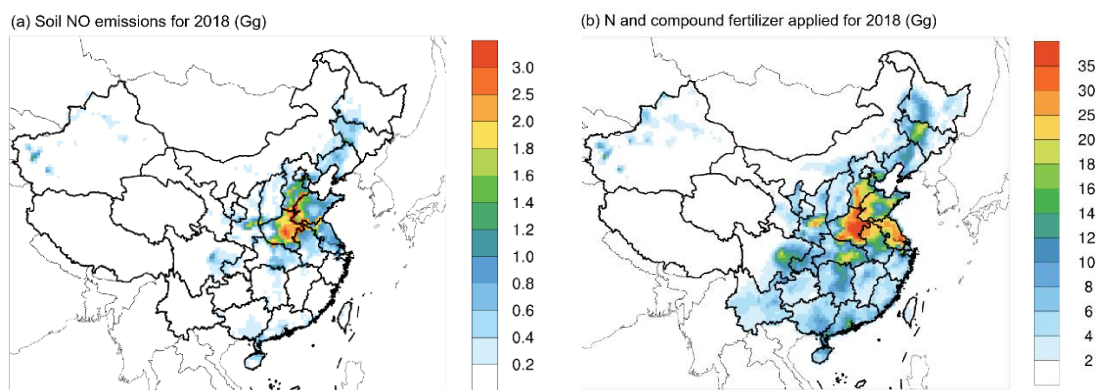
186 In this study, two methods were used to quantify the impact of soil NO emissions on surface  
187 ozone concentration during the simulation period. The first is the conventional brute-force  
188 method (BFM), which involves comparing the simulated ozone concentration between the  
189 base case and a scenario case without soil NO emissions. The difference between these two  
190 scenarios was considered to represent the contribution of soil NO emissions to ozone. The  
191 second method applies the widely used Ozone Source Apportionment Technology (OSAT)  
192 implemented in CAMx (Yarwood et al., 1996), with soil NO emissions being tagged as an  
193 individual emission group. OSAT attributes ozone formation to NO<sub>x</sub> or VOCs based on their  
194 relative availability and apportions NO<sub>x</sub> and VOCs emissions by source group/region  
195 (Ramboll, 2021). In addition to soil NO emissions, anthropogenic and natural emissions  
196 (including biogenic VOC emissions, lightning NO emissions, and open biomass burning)  
197 were also tagged as individual emission groups.

198 **3. Results and discussions**

199 3.1. Soil NO emissions for 2018 in China

200 3.1.1. Spatial and temporal variations

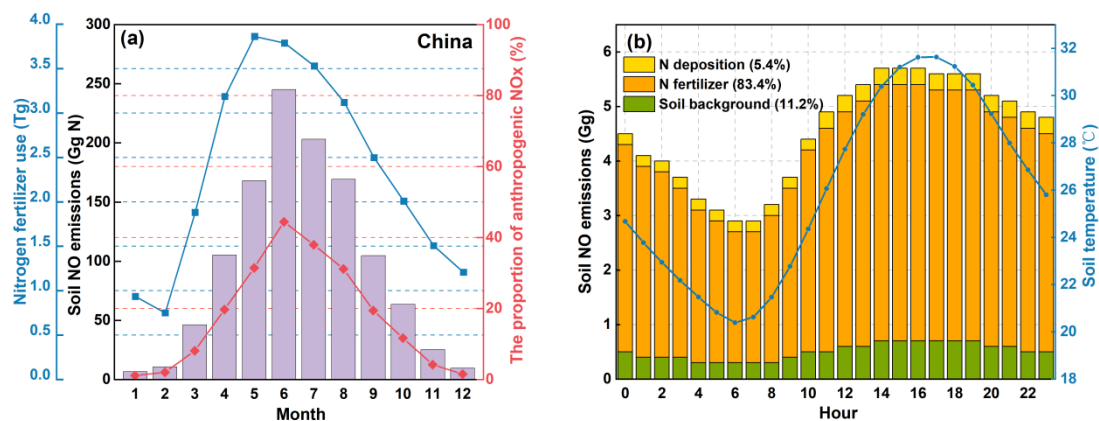
201 National total soil NO emissions for 2018 is estimated to be 1157.9 Gg N, with an uncertainty  
202 range of 715.7~1902.6 Gg N, which will be discussed more in Section 3.1.2. On an annual  
203 scale, soil NO emissions accounted for 17.3% of the total anthropogenic NO<sub>x</sub> emissions in  
204 China for 2017 (based on MEIC inventory). This ratio varies from 12.0% to 35.3% at regional  
205 scale. Unlike the anthropogenic NO<sub>x</sub> emissions that concentrate over densely populated  
206 regions (e.g., NCP, YRD), soil NO emissions are most abundant in Central China, particularly  
207 Henan Province and nearby provinces, including Hebei and Shandong in the NCP, Jiangsu  
208 and Anhui in northern YRD (Fig. 2a). Other hotspots of soil NO emissions include Northeast  
209 China and the eastern part of the Sichuan Basin. As expected, the spatial distribution of soil  
210 NO emissions closely mirrors that of the fertilizer application (Fig. 2b). Henan (located in  
211 Central China), Shandong (NCP), and Hebei (NCP) are the top three provinces that have the  
212 highest fertilizer application (together accounting for 24.1% of national totals in 2018) and  
213 thus highest soil NO emissions (together accounting for 35.7%).



214 **Figure 2.** Spatial distribution of (a) soil NO emissions for 2018 and (b) N and compound  
215 fertilizer applied for 2018.

216 In terms of the monthly variations, the total soil NO emissions show a unimodal pattern (as  
217 shown in Fig. 3a with the highest emissions occurring in the summer months of June, July,  
218 and August), except for South China and Southeast China (Fig. S2), where the peak emissions  
219 occur in April or May. Soil NO emissions during the summer months account for 28.2%  
220 (South China) to 67.6% (Northeast China) of the annual totals (Fig. 1 and Table S5). The  
221 shape of monthly soil NO emissions is influenced by temperature and the timing of fertilizer  
222 application. The BDSNP algorithm assumes that 75% of the annual fertilizer is applied over  
223 the first month of the growing season, with the remaining 25% applied evenly throughout the  
224 rest of the growing season. This assumption results in a significant amount of fertilizer being

225 applied from April to August (Fig. 3a). In contrast, anthropogenic  $\text{NO}_x$  emissions display  
 226 weaker monthly variations (Zheng et al., 2021). Consequently, the ratio of soil NO emissions  
 227 to anthropogenic  $\text{NO}_x$  (SN/ $\text{AN}$ ) is much higher during the summer months. In regions such as  
 228 Central China and Northwest China, where soil NO emissions are high and anthropogenic  
 229  $\text{NO}_x$  emissions are relatively low, SN/ $\text{AN}$  reaches 74.0% and 67.5% during the summer  
 230 months (Fig. 1 and Table S5). In East China and North China, where anthropogenic  $\text{NO}_x$   
 231 emissions are high, SN/ $\text{AN}$  ranges from 26.8% to 36.5% during the summer months. These  
 232 findings are align with Chen et al. (2022), who reported that soil NO emissions made up 28%  
 233 of total  $\text{NO}_x$  (soil NO + anthropogenic  $\text{NO}_x$ ) emissions in summer and could reach 50–90% in  
 234 isolated areas and suburbs. The substantial contribution of soil NO emissions during the  
 235 ozone pollution season implies a potentially significant impact on surface ozone  
 236 concentration. In terms of diurnal variations, soil NO emissions peak in the afternoon due to  
 237 diurnal temperature fluctuations. As illustrated by Fig. 3b, the average hourly soil NO  
 238 emissions over NCP for June 2018 closely follow the WRF simulated temperature changes.  
 239 The BDSNP algorithm identifies three sources of soil nitrogen: background, atmospheric  
 240 nitrogen deposition, and fertilizer application, with the latter being the primary contributor. A  
 241 decomposition analysis of soil NO emissions for NCP reveals that fertilizer application  
 242 accounts for 83.4% of total NO soil emissions (Fig. 3b), while background and atmospheric  
 243 nitrogen deposition only contribute for 11.2% and 5.4%, respectively. Thus, although soil NO  
 244 emissions are generally considered a “natural” source (Galbally et al., 2008) and are not  
 245 currently targeted in  $\text{NO}_x$  emission mitigation strategies, human fertilizer activities render soil  
 246 NO emissions an anthropogenic source.



247 **Figure 3.** (a) Monthly fertilizer (N + compound) applied and soil NO emissions in China and  
 248 (b) hourly soil NO emissions for 2018 June in NCP and domain-averaged soil temperature  
 249 simulated by WRF.

### 250 3.1.2. Limitations and uncertainties associated with soil NO emission estimation

251 Although the current BDSNP algorithm is considered more sophisticated than the old YL95



252 algorithm, it still suffers certain limitations. For example, the current BDSNP  
253 parameterization employs a static classification of “arid” versus “non-arid” soils, upon which  
254 the relationship between soil NO emissions and soil moisture relies (Hudman et al., 2012).  
255 However, recent studies (Sha et al., 2021; Huber et al., 2023) have shown more dynamic  
256 representation of this classification is needed to capture the emission characteristics as  
257 observed by many chamber and atmospheric studies (e.g., Oikawa et al. (2015); Huang et al.  
258 (2022a)). Huber et al. (2023) also showed that the emission estimated based on the static  
259 classification are very sensitive to the soil moisture and thus could not produce self-consistent  
260 results when using different soil moisture products.

261 In addition to the aforementioned limitation, the estimated soil NO emissions are also  
262 subjected to certain limitations and large uncertainties. The first uncertainty comes from the  
263 amount of fertilizer application, which has been identified as the dominant contributor to soil  
264 NO emissions, as mentioned above. According to the global dataset (Potter et al., 2010), the  
265 amount of fertilizer applied is 19.6 Tg, which is comparable to the sum of nitrogen fertilizer  
266 for 2018 (20.7 Tg) obtained from provincial statistical yearbooks. However, compound  
267 fertilizer, usually with a nitrogen, phosphorus, and potassium ratio of 15: 15: 15, has been  
268 used more in China. Each number represents the percentage of the nutrient by weight in the  
269 fertilizer. In the case of 15:15:15 NPK fertilizer, it means that the fertilizer contains 15%  
270 nitrogen, 15% phosphorus, and 15% potassium. Since 2016, the amount of nitrogen fertilizer  
271 has been decreasing annually at an average rate of 4.6%, while the amount of compound  
272 fertilizer has been increasing since 2010 at an average rate of 3.3%. The ratio of compound  
273 fertilizer to nitrogen fertilizer has increased from 76.4% in 2010 to 109.8% in 2018.  
274 Consequently, soil NO emissions may be largely underestimated if the compound fertilizer is  
275 not taken into account. Our calculation shows that if only nitrogen fertilizer is considered, the  
276 estimated total soil NO emissions are 805.2 Gg N/a for 2018, which is comparable to the  
277 value (770 Gg N/a averaged during 2008-2017) reported by Lu et al. (2021), but 30.5% lower  
278 than that based on both nitrogen fertilizer and compound fertilizer. Regionally, this  
279 underestimation ranges from 11.1%~41.5%, with a larger underestimation in Central China  
280 and East China (Fig. S3).

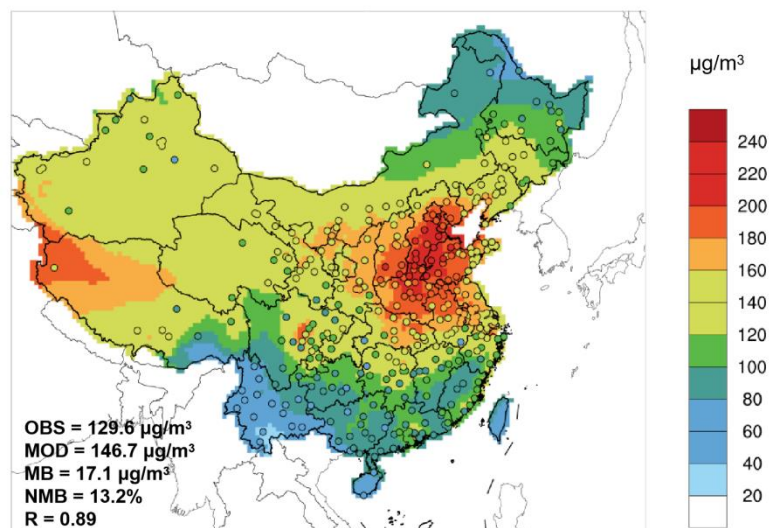
281 Another major uncertainty in estimating soil NO emissions is the temperature dependence  
282 factor  $f(T)$  in Eq.1. According to the BDSNP scheme, soil NO emissions increase  
283 exponentially with temperature between 0 and 30°C and reach a maximum when the  
284 temperature exceeds 30°C. The default temperature dependence coefficient (i.e.,  $k$  in Eq. S2)  
285 follows the value used in the YL95 scheme, which is  $0.103\pm 0.04$ . However, as shown by  
286 Table 3 in Yienger and Levy (1995), this value is the weighted average of values reported for  
287 different land types, which shows a wide range from 0.040 to 0.189. Even for the same crop  
288 type (e.g., corn), the value of  $k$  could be quite different (0.130 vs. 0.066). We conducted a

289 sensitivity analysis to examine the impact of varying the  $k$  value on estimated soil NO  
290 emissions. When the  $k$  value decreases or increases by 20%, the estimated total soil NO  
291 emissions change from 715.7 to 1902.6 Gg N/a, representing a relative difference of -  
292 38.2~64.3% deviation from the default value (1157.9 Gg N/a). Using the default  $k$  value  
293 would result in a large overestimation of simulated NO<sub>2</sub> concentrations over NCP and YRD  
294 and underestimation over Northeast China (Fig. S4). According to the total sown areas of  
295 farm crops reported in the provincial statistical yearbook, the primary crops grown in these  
296 regions are wheat and corn, which have a relatively low  $k$  value (0.066~0.073). Therefore, we  
297 adjusted  $k$  for NCP (reduced by 20%), YRD (reduced by 10%), and Northeast China  
298 (increased by 10%). CAMx simulation results show that this adjustment would not  
299 significantly affect the simulated MDA8 O<sub>3</sub> concentration but could reduce the NO<sub>2</sub> gap  
300 between observation and simulation (Fig. S4-S5). Therefore, we applied this adjustment to  
301 soil NO emissions in the following CAMx simulations.

## 302 3.2. Contribution of soil NO emissions to ground-level ozone

### 303 3.2.1. Base case model evaluation

304 Fig. 4 shows the monthly averaged MDA8 ozone concentration simulated for June 2018 with  
305 observed values presented on top. Overall the model well captured the spatial distribution of  
306 MDA8 with a spatial correlation  $R = 0.89$ . Over the 365 cities in China, the simulated  
307 monthly averaged MDA8 ozone concentration is  $146.7 \pm 36.1 \mu\text{g}/\text{m}^3$ , which is slightly higher  
308 than the observed value of  $129.6 \pm 37.6 \mu\text{g}/\text{m}^3$  (NMB = 13.2%). Regionally, model shows  
309 better performance in Northeast China (MB =  $2.4 \mu\text{g}/\text{m}^3$ , NMB = 1.9%) and NCP (MB =  $13.3$   
310  $\mu\text{g}/\text{m}^3$ , NMB = 7.7%). Over-prediction is observed for Sichuan Basin and YRD (Table S6).  
311 Simulated ozone concentration over the northwest Qinghai-Tibet Plateau was also much  
312 higher than observed values. Our OSAT results (shown later) show that the high ozone  
313 concentration over the Qinghai-Tibet Plateau is mostly contributed by the transport of  
314 boundary ozone, which includes both horizontal and vertical (i.e., stratosphere) directions. For  
315 regions with high altitude (e.g., the Qinghai-Tibet Plateau), vertical ozone intrusion from the  
316 stratosphere is most substantial, which is consistent with the finding by Chen et al. (2023) that  
317 the boundary layer height was identified as the most important feature for ozone over the  
318 Qinghai-Tibet Plateau.



319

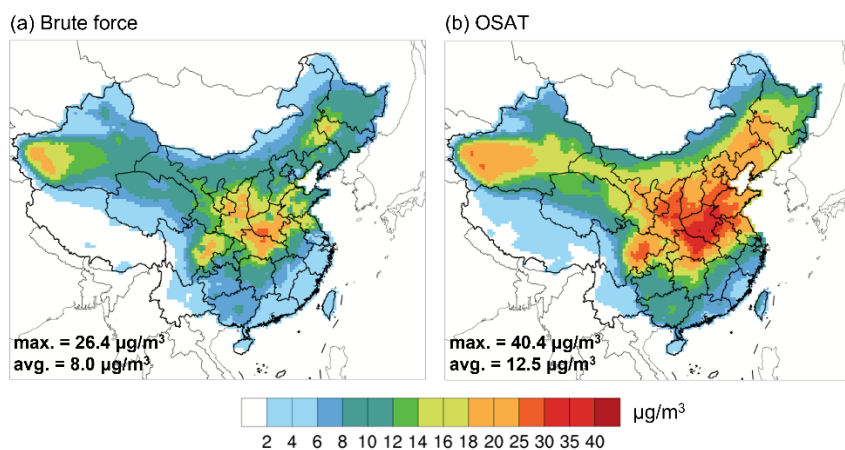
320 **Figure 4.** Comparison of simulated (base colors) and observed (scatter points) values of  
 321 MDA8 ozone in June 2018.

### 322 3.2.2. Impacts on regional ozone

323 To assess the contribution of soil NO emissions to surface ozone, both the brute-force method  
 324 (BFM) and the OSAT method were applied, and the results are shown in Fig. 5. Generally, the  
 325 two methods show consistent ozone contribution from soil NO emissions but with different  
 326 magnitudes. The BFM method shows widespread ozone enhancement due to soil NO  
 327 emissions with a spatial pattern that aligns with the distribution of soil NO emissions.  
 328 Substantial ozone enhancement is found over Central China, Sichuan Basin, northern YRD,  
 329 and eastern Northeast China. Maximum ozone enhancement ( $\Delta$ MDA8) due to soil NO  
 330 emissions is  $26.4 \mu\text{g}/\text{m}^3$  with a domain-average value of  $8.0 \mu\text{g}/\text{m}^3$ . For selected key regions,  
 331 the ozone contribution ranges from low to high: PRD ( $3.8 \pm 1.1 \mu\text{g}/\text{m}^3$ ), YRD ( $8.7 \pm 4.7$   
 332  $\mu\text{g}/\text{m}^3$ ), Sichuan Basin ( $9.1 \pm 0.9 \mu\text{g}/\text{m}^3$ ), Northeast ( $9.3 \pm 3.0 \mu\text{g}/\text{m}^3$ ), and NCP ( $13.9 \pm 4.4$   
 333  $\mu\text{g}/\text{m}^3$ ), respectively. A similar spatial pattern is observed with the OSAT results, but the  
 334 magnitudes are much higher. Maximum ozone contribution by soil NO emissions reaches  
 335  $40.4 \mu\text{g}/\text{m}^3$  according to OSAT results, which is 53.0% higher than the brute force method.  
 336 The corresponding ozone contribution for each selected region is  $6.7 \pm 1.2 \mu\text{g}/\text{m}^3$  (PRD),  $13.5$   
 337  $\pm 7.4 \mu\text{g}/\text{m}^3$  (Sichuan Basin),  $14.5 \pm 4.9 \mu\text{g}/\text{m}^3$  (Northeast China),  $16.2 \pm 7.8 \mu\text{g}/\text{m}^3$  (YRD)  
 338 and  $25.7 \pm 5.3 \mu\text{g}/\text{m}^3$  (NCP). The scatter plots between BFM and OSAT results show good  
 339 correlations (Fig. S6,  $R^2 = 0.78\text{--}0.97$ ), with OSAT results higher by 10%~61%. For YRD,  
 340 Sichuan Basin, and Northeast, the difference between the OSAT method and BFM increases  
 341 with the absolute ozone concentration (Fig. S7), while NCP shows the opposite trend. The  
 342 difference between the two methods reflects the nonlinear ozone response to  $\text{NO}_x$  emissions.  
 343 This nonlinearity becomes stronger in regions with larger  $\text{NO}_x$  concentrations, especially  
 344 where  $\text{O}_3$  production is characterized as  $\text{NO}_x$ -saturated (or VOC-limited), such as the NCP. In

345 such cases, removing a portion of the NO emissions (e.g., zeroing out soil NO for the BFM  
 346 simulation) makes O<sub>3</sub> production from the remaining NO emissions more efficient, which  
 347 lessens the O<sub>3</sub> response. As shown later in Figure 7a, the O<sub>3</sub> response for NCP is more curved  
 348 (nonlinear) than other regions, consistent with NCP tending to have more NO<sub>x</sub>-saturated O<sub>3</sub>  
 349 production. This nonlinear effect also explains smaller O<sub>3</sub> attribution to soil NO by the BFM  
 350 than OSAT, especially over the NCP. Attributing a secondary pollutant to a primary emission  
 351 (e.g., O<sub>3</sub> to NO) is inherently tricky with nonlinear chemistry, as Koo et al. (2009) discussed.  
 352 Therefore, it is useful to present estimates from different methods. The Path Integral Method  
 353 (PIM) is a source apportionment method that explicitly treats nonlinear responses with  
 354 mathematical rigor (Dunker et al., 2015). However, applying the PIM is more costly than the  
 355 BFM or OSAT.

356 In addition to soil NO contribution, OSAT also gives ozone contributions from other source  
 357 groups, including anthropogenic emissions within China, boundary contribution, natural  
 358 emissions (e.g., biogenic emissions, open biomass burning, lightning NO<sub>x</sub>), and emissions  
 359 outside China. The spatial distribution for each source category is presented in Fig. S8, and  
 360 the relative contribution for each selected region is shown in Fig. S9. Overall, boundary  
 361 transport (56.5%) and anthropogenic emissions (24.0%) contribute most to MDA8 ozone for  
 362 June 2018. Boundary contribution is high over the western and northern parts of China, while  
 363 the contribution from anthropogenic emissions is substantial over eastern China, where  
 364 anthropogenic emissions are extensive. On a national scale, soil NO emissions exhibit a  
 365 relative ozone contribution of 9.1%, and regionally this value ranges from 6.1% in PRD to  
 366 13.8% in NCP.



367  
 368 **Figure 5.** Ozone contribution from soil NO emissions based on (a) brute force method and (b)  
 369 OSAT method.

370 We further evaluated the impact of soil NO emissions on the number of ozone exceedances  
 371 days (i.e., days with MDA8 O<sub>3</sub> higher than 160 µg/m<sup>3</sup>) during June 2018 based on the relative  
 372 response factor (RRF) method and results from the brute force method. The total number of

373 ozone exceedances days during June 2018 for the five selected regions ranged from 50 days  
 374 in PRD to 985 days in NCP (Table 1). The number of ozone exceedance days per city ranged  
 375 from 3.1 days in Sichuan Basin to 18.2 days in NCP, suggesting the severe ozone pollution in  
 376 June 2018 over NCP. RRF was first calculated for each city as the ratio of simulated ozone  
 377 concentration between the base case and the case with soil NO emissions excluded and  
 378 applied to the observed ozone concentrations to obtain adjusted ozone concentrations without  
 379 soil NO emissions. Soil NO emissions are estimated to lead to 121 ozone exceedance days in  
 380 NCP, followed by 84 days in the Northeast and 70 days in YRD, corresponding to a percent  
 381 change of 12.3%, 32.8%, and 10.5%, respectively. In Sichuan Basin, where soil NO emissions  
 382 are also substantial, soil NO emissions contribute 30 ozone exceedances days, which accounts  
 383 for 43.5% of the total ozone exceedances days. These results suggest the substantial  
 384 contribution of soil NO emissions to the number of ozone pollution days over regions with  
 385 high soil NO emissions.

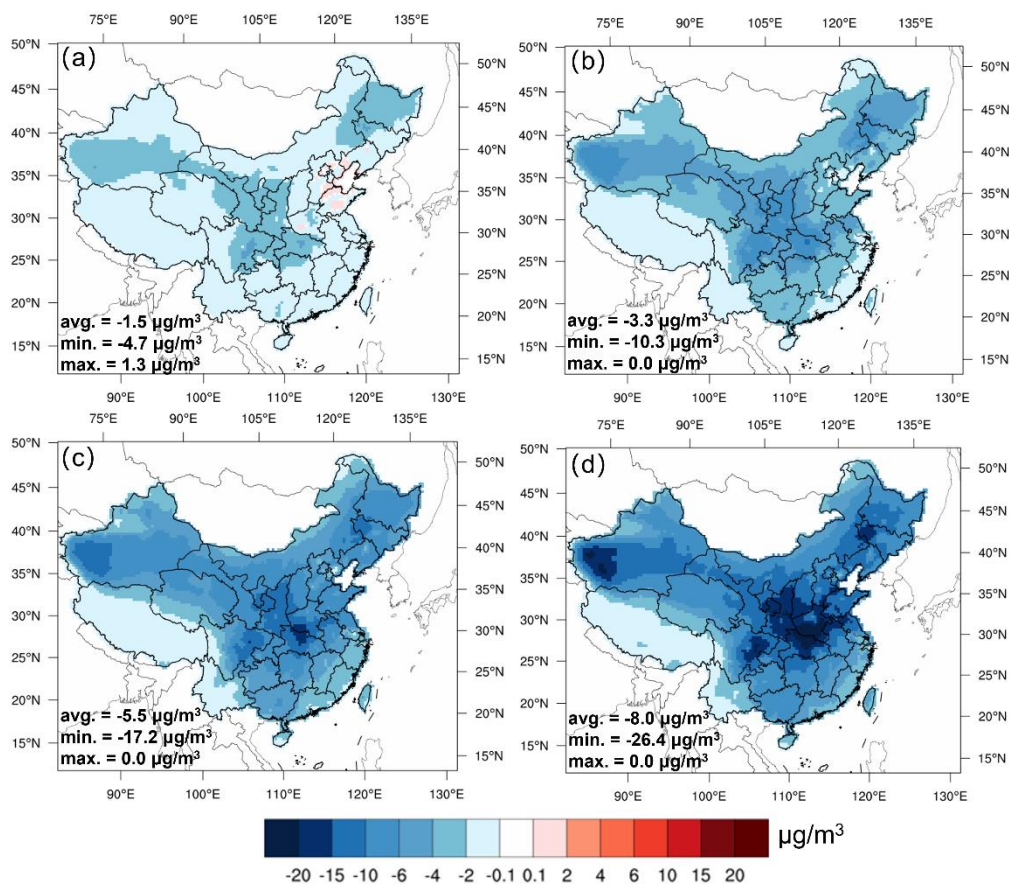
386 **Table 1.** Number of ozone exceedances over selected regions during June 2018.

Region (No. of cities)	Number of ozone exceedance days (% of total days)	$\Delta$ ozone exceedances days when soil NO emissions are removed	% of total ozone exceedances days
NCP (54)	985 (60.8%)	-121	-12.3%
YRD (55)	666 (41.1%)	-70	-10.5%
PRD (9)	50 (18.5%)	-6	-12.0%
Sichuan Basin (22)	69 (10.5%)	-30	-43.5%
Northeast (37)	256 (23.1%)	-84	-32.8%

### 387 3.3. Ozone responses to reductions in soil NO emissions

388 Current NO<sub>x</sub> emission control policies primarily target combustion sources, such as power  
 389 plants (Du et al., 2021) and on-road vehicles (Park et al., 2021). Nitrification inhibitors, such  
 390 as dicyandiamide (DCD, C<sub>2</sub>H<sub>4</sub>N<sub>4</sub>), have been found to be effective in reducing nitrogen loss,  
 391 thereby reducing NO emissions from soil (Abalos et al., 2014). Studies have shown that using  
 392 5% DCD with nitrogen fertilizer can reduce NO emissions by up to 70% (Xue et al., 2022). In  
 393 light of this, it is important to evaluate the impact of reduced soil NO emissions on ozone  
 394 concentration. To address this question, four sensitivity simulations were carried out for June  
 395 2018, with soil NO emissions reduced by 25%, 50%, 75%, and 100% relative to the base  
 396 case. As shown by Fig. 6, reducing soil NO emissions led to a general decrease in monthly  
 397 MDA8 ozone concentration ( $\Delta$ MDA8), with the magnitude of  $\Delta$ MDA8 becoming more  
 398 significant with the reduction ratio. With a 25% reduction in soil NO emissions, there was a  
 399 widespread small decrease in monthly average MDA8 ozone concentration ( $\Delta$ MDA8: -  
 400  $1.5 \pm 0.9 \mu\text{g}/\text{m}^3$ ), except over NCP where ozone showed a slight increase (up to  $1.3 \mu\text{g}/\text{m}^3$ ) in  
 401 Shandong and Henan province. **These ozone increases reflect the nonlinearity of ozone**

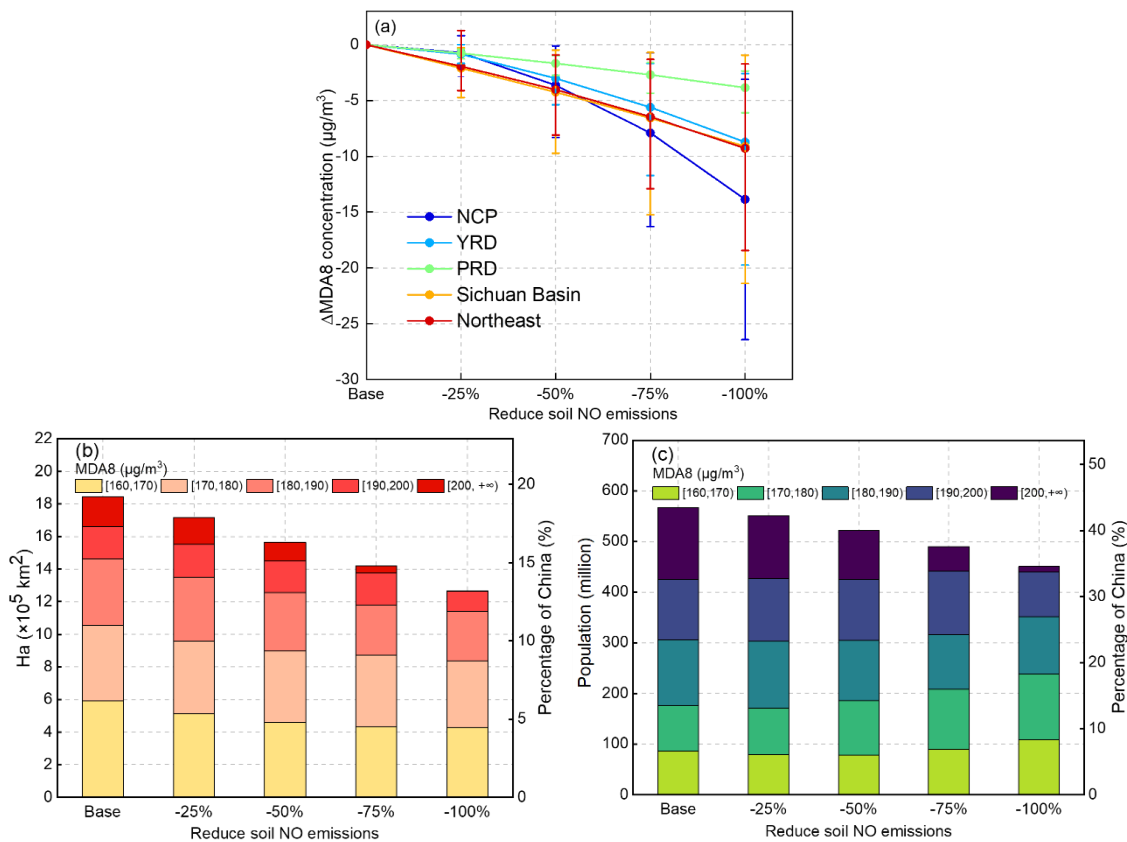
402 chemistry and this nonlinearity becomes stronger in regions with large  $\text{NO}_x$  concentrations,  
 403 especially where  $\text{O}_3$  production is characterized as VOC-limited (such as NCP). When soil  
 404  $\text{NO}$  emissions were cut by 50%, the effect of reduced  $\text{O}_3$  titration is overwhelmed by reduced  
 405  $\text{O}_3$  formation due to less  $\text{NO}_x$  available, thus the  $\Delta\text{MDA8}$  showed a ubiquitous decrease across  
 406 entire China with an average  $\Delta\text{MDA8}$  of  $-5.5 \mu\text{g}/\text{m}^3$ . When soil  $\text{NO}$  emissions were removed  
 407 entirely, the maximum  $\Delta\text{MDA8}$  could exceed  $25 \mu\text{g}/\text{m}^3$  over central China, part of the  
 408 Sichuan Basin, Northeast China, and Northeast China. Regions with strong ozone responses  
 409 generally aligned with regions that also had high soil  $\text{NO}$  emissions. However, it should be  
 410 noted that the ozone response to soil  $\text{NO}$  reductions not only depends on the magnitude of soil  
 411  $\text{NO}$  emissions but is also affected by (1) the local ozone formation regime that is further  
 412 determined by the relative abundance of  $\text{NO}_x$  and VOCs, and (2) changes in transport of  
 413 upwind ozone.



414  
 415 **Figure 6.** Spatial distribution of  $\Delta\text{MDA8}$  under (a) 25%, (b) 50%, (c) 75%, and (d) 100%  
 416 reductions of soil  $\text{NO}$  emissions in June 2018.

417 Fig. 7a provides further details on the domain-averaged  $\Delta\text{MDA8}$  under different reduction  
 418 scenarios for the five key regions. As expected, the ozone response in each region increased as the  
 419 reduction in the soil  $\text{NO}$  emissions increased. NCP exhibited the strongest ozone responses to  
 420 changes in soil  $\text{NO}$  emissions, with  $\Delta\text{MDA8}$  increasing from  $-0.7 \pm 0.8 \mu\text{g}/\text{m}^3$  with 25% reductions

421 to  $-13.9 \pm 4.4 \mu\text{g}/\text{m}^3$  when all soil NO emissions were removed. YRD, Sichuan Basin, and  
 422 Northeast China exhibit similar ozone responses when soil NO emissions are reduced. Under the  
 423 25% scenario,  $\Delta\text{MDA8}$  ranged from  $-4.7$  to  $1.3 \mu\text{g}/\text{m}^3$  for these three regions; with 100% soil NO  
 424 reductions,  $\Delta\text{MDA8}$  ranged from  $-21.4$  to  $-0.9 \mu\text{g}/\text{m}^3$ .  $\Delta\text{MDA8}$  in PRD was relatively small. Even  
 425 with a 100% reduction, the average  $\Delta\text{MDA8}$  in PRD was less than  $5 \mu\text{g}/\text{m}^3$ , which is associated  
 426 with the small soil NO emissions in PRD. It is interesting to note that all regions except NCP  
 427 exhibited an approximate linear ozone response to changes in soil NO emission reductions. NCP  
 428 showed more significant ozone reductions as the reduction ratio increased, suggesting that NCP  
 429 would gain more benefits with more aggressive reductions in soil NO emissions compared to other  
 430 regions.



431 **Figure 7.** (a)  $\Delta\text{MDA8}$  concentrations in five key regions under different emission reduction  
 432 scenarios (b) Area and (c) population exposed to different ozone levels under different soil  
 433 NO emission reduction scenarios.

434 We evaluated the impact of different soil NO emission reduction scenarios on the area and  
 435 population exposed to varying ozone levels. The results, presented in Fig. 7b and 7c, revealed  
 436 a decrease in coverage and exposed population under high ozone concentrations as soil NO  
 437 emissions decrease. The data presented in the plots are for grid cells with monthly MDA8  
 438 ozone concentrations exceeding  $160 \mu\text{g}/\text{m}^3$ . In the Base scenario, the estimated coverage of  
 439 MDA8 ozone exceeding  $160 \mu\text{g}/\text{m}^3$  was  $1.84 \times 10^6 \text{ km}^2$ , equivalent to 19.2% of the national

440 land area. The population exposed to ozone concentrations exceeding  $160 \mu\text{g}/\text{m}^3$  amounts to  
441 566.6 million, representing 43.4% of the entire population. The areas with extremely high  
442 ozone concentrations ( $\text{MDA8} > 200 \mu\text{g}/\text{m}^3$ ) account for 1.9% of the national land area, with a  
443 corresponding exposed population of 10.9%, indicating that densely populated areas  
444 experience higher ozone concentrations. When soil NO emissions are halved, there is a 15.2%  
445 reduction in the coverage of non-attainment areas and an 8.0% reduction in the total exposed  
446 population. If soil NO emissions are eliminated, the total area coverage and population  
447 exposed to MDA8 ozone concentrations exceeding  $160 \mu\text{g}/\text{m}^3$  would be  $1.27 \times 10^6 \text{ km}^2$  and  
448 450.3 million, respectively, representing 13.2% and 34.5% of the total. Compared to the Base  
449 scenario, a 100% theoretical reduction in soil NO emissions leads to a 31.3% and 20.5%  
450 reduction in the exposed area and population under high ozone concentration, respectively,  
451 indicating substantial health benefits gained when soil NO emissions are mitigated.

452 Fig. S10-S11 displays similar area and population plots for selected key regions. The overall  
453 trends for each sub-region are consistent. With 100% reductions in soil NO emissions, the  
454 area with high ozone concentration decreased by 17.8%, 22.3%, 65.4%, and 100% for NCP,  
455 YRD, Sichuan Basin, and Northeast. The corresponding values for the exposed population are  
456 91.4%, 60.3%, 9.8%, and 0.0%. While the relative change is more significant in Sichuan  
457 Basin and Northeast China, NCP and YRD gain more health benefits due to the significantly  
458 higher total population for these two regions. However, it is worth noting that even with the  
459 complete elimination of soil NO emissions, a total of 450.3 million people are still exposed to  
460 ozone levels exceeding the national standard, necessitating multiple control policies at the  
461 same time, such as synergistic control of anthropogenic VOC emissions (Chen et al., 2022;  
462 Ding et al., 2021).

### 463 3.4 Comparison with existing studies

464 The soil NO emissions estimated in this study were also compared with values reported by  
465 existing studies based on either field measurement or model estimation (Table S7). Previous  
466 studies report a wide range of soil NO emissions from 480 to 1375 Gg N and soil NO flux  
467 ranging from 10 to  $47.5 \text{ ng N m}^{-2} \text{ s}^{-1}$ . The soil NO emissions estimated in our study are 1157.9  
468 Gg N with the default  $k$  value and 951.9 Gg N with region-adjusted  $k$  value, which falls  
469 within the upper range of previously reported values. The averaged soil NO flux over NCP in  
470 June 2018 estimated in our study is  $35.4 \text{ ng N m}^{-2} \text{ s}^{-1}$ , which is within the range reported by  
471 previous studies ( $12.9\text{--}40.0 \text{ ng N m}^{-2} \text{ s}^{-1}$ ).

472 The simulated ozone contribution by soil NO emissions is compared with other studies. In  
473 California, soil NO was estimated to cause a 23.0% increase in surface  $\text{O}_3$  concentrations (Sha  
474 et al., 2021). Constrained by satellite measured  $\text{NO}_2$  column densities, Wang et al. (2022b)  
475 reported MDA8 ozone contribution of  $9.0 \mu\text{g}/\text{m}^3$  (relative contribution of 5.4%) from



476 cropland NO<sub>x</sub> emissions over NCP during a growing season in 2020. Lu et al. (2021) showed  
477 an interactional effect of domestic anthropogenic emissions with soil NO emissions of 9.5 ppb  
478 in the NCP during July 2017. In addition, soil NO<sub>x</sub> emissions strongly affect the sensitivity of  
479 ozone concentrations to anthropogenic sources in the NCP. In a most recent study by Shen et  
480 al. (2023), addition of the soil NO<sub>x</sub> emissions was shown to result in up to 15 ppb increase of  
481 ozone concentration over Xinjiang, Tibet, Inner Mongolia, and Heilongjiang, although a  
482 minor reduction was evident over the Yangtze River basin. The findings of this study align  
483 with previous studies, emphasizing the important role of soil NO emissions in influencing  
484 surface ozone concentrations in China. Furthermore, spatial heterogeneities exist in terms of  
485 both the soil NO emissions and the responses of ozone to reductions in soil NO emissions.  
486 However, it should be noted that the spatial pattern of ozone response to reduced soil NO  
487 emissions in this study is different from Shen et al. (2023). For instance, with a 30% reduction  
488 in soil NO emissions, O<sub>3</sub> concentration increased by 3-5 ppb over Inner Mongolia,  
489 Heilongjiang, Xinjiang, and Tibet and decreased by 0-2 ppb over the Yangtze River basin in  
490 Shen et al. (2023). In this study, a 20% reduction in soil NO emissions was found to lead to  
491 widespread but small decrease (less than 4 μg/m<sup>3</sup>) in ozone concentrations except the NCP  
492 (Fig. 6a). These inconsistencies may stem from the differences in the estimated soil NO  
493 emissions, both associated with the magnitude and the spatial distribution, as also noted in  
494 other study (Zhu et al., 2023). Therefore, more observations, such as direct measurement of  
495 soil NO flux, especially over agricultural areas, are urgently needed to better constrain the  
496 estimated soil NO emissions.

#### 497 **4. Conclusions**

498 Soil NO emissions are non-negligible NO<sub>x</sub> sources, particularly during summer. The  
499 importance of soil NO emissions to ground-level ozone in China is much less evaluated than  
500 combustion NO<sub>x</sub> emissions. In this study, the total national soil NO emissions were estimated  
501 to be 1157.9 Gg N in 2018 based the BDSNP algorithm, with a spatial distribution closely  
502 following that of fertilizer application. High soil NO emissions were greatest over Henan,  
503 Shandong, and Hebei provinces, which differs significantly from where anthropogenic NO<sub>x</sub>  
504 emissions are. Distinct diurnal and seasonal variations in soil NO emissions were found,  
505 mainly driven by the changes in soil temperature as well as the timing of fertilizer application.  
506 Uncertainty analysis of the estimated soil NO emissions reveals a range of 715.7~1902.6 Gg  
507 N that warrants further study and, preferably, constraint from observations.

508 Using two ozone source attribution methods (BFM and OSAT), we evaluated the contribution  
509 of soil NO emissions to ground-level ozone concentration for June 2018. Both methods  
510 suggest a substantial contribution of soil NO emissions to MDA8 ozone concentrations of  
511 8~12.5 μg/m<sup>3</sup> on average for June 2018, with the OSAT results consistently higher than BFM.

512 Soil NO emissions were shown to increase of ozone exceedances days (i.e., MDA8 above 160  
513  $\mu\text{g}/\text{m}^3$ ) by 10.0%~43.5% depending on region. Reducing soil NO emissions could generally  
514 reduce the ground-level ozone concentrations and population exposure to unhealthy ozone  
515 levels, especially over NCP and YRD. For example, a 50% reduction in soil NO emissions  
516 decreased land area experiencing ozone above 160  $\mu\text{g}/\text{m}^3$  by 15.2% and the population  
517 exposed to this ozone concentration by 8.0%. However, even with complete removal of soil  
518 NO emissions, approximately 450.3 million people are still exposed to ozone above 160  
519  $\mu\text{g}/\text{m}^3$ .

520 The major findings of this study reinforce previous studies by highlighting the important  
521 contribution of soil NO emissions to surface ozone concentrations in China, although  
522 substantial uncertainties remain with soil NO emission estimates. Observational constraints  
523 on the magnitude of soil  $\text{NO}_x$  emissions in China are needed. Ozone response to reducing soil  
524 NO emissions varies by region due to the non-linear chemistry of ozone formation. Future  
525 ozone mitigation strategies should consider the potential benefit of reducing non-combustion  
526  $\text{NO}_x$  emissions, such as soil NO, with due consideration to the sensitivity of ozone to reducing  
527  $\text{NO}_x$  in the region.

528 **Data availability.** Data will be made available on request.

529 **Author contributions.** **Ling Huang:** Conceptualization, Formal analysis, Writing – original  
530 draft. **Jiong Fang:** Data curation, Formal analysis, Visualization. **Jiaqiang Liao:** Data  
531 curation, Formal analysis, Visualization. **Greg Yarwood:** Writing – review & editing. **Hui**  
532 **Chen:** Writing – review & editing. **Yangjun Wang:** Writing – review & editing. **Li Li:**  
533 Conceptualization, Supervision, Funding acquisition.

534 **Competing interests.** The authors declare that they have no known competing financial  
535 interests or personal relationships that could have appeared to influence the work reported in  
536 this paper.

537 **Acknowledgments.** This study was financially sponsored by the National Natural Science  
538 Foundation of China (grant No. 42005112, 42075144), the Open Funding of Zhejiang Key  
539 Laboratory of Ecological and Environmental Big Data (No. EEED-2022-06), the Shanghai  
540 International Science and Technology Cooperation Fund (No.19230742500). This work is  
541 supported by Shanghai Technical Service Center of Science and Engineering Computing,  
542 Shanghai University.

## 543 **References**

544 Abalos, D., Jeffery, S., Sanz-Cobena, A., Guardia, G., and Vallejo, A.: Meta-analysis of the effect of  
545 urease and nitrification inhibitors on crop productivity and nitrogen use efficiency, *Agriculture,*  
546 *Ecosystems & Environment*, 189, 136-144, 2014.  
547 Almaraz, M., Bai, E., Wang, C., Trousdell, J., Conley, S., Faloona, I., and Houlton, B. Z.: Agriculture is  
548 a major source of  $\text{NO}_x$  pollution in California, *Science advances*, 4, eaao3477, 2018.

549 Cakaj, A., Qorri, E., Coulibaly, F., De Marco, A., Agathokleous, E., Leca, S., and Sicard, P.: Assessing  
550 surface ozone risk to human health and forests over time in Poland, *Atmospheric Environment*, 119926,  
551 2023.

552 Chang, J., Brost, R., Isaksen, I., Madronich, S., Middleton, P., Stockwell, W., and Walcek, C.: A three -  
553 dimensional Eulerian acid deposition model: Physical concepts and formulation, *Journal of*  
554 *Geophysical Research: Atmospheres*, 92, 14681-14700, 1987.

555 Chen, B., Wang, Y., Huang, J., Zhao, L., Chen, R., Song, Z., and Hu, J.: Estimation of near-surface  
556 ozone concentration and analysis of main weather situation in China based on machine learning model  
557 and Himawari-8 TOAR data, *Science of The Total Environment*, 864, 160928, 2023.

558 Chen, W., Guenther, A. B., Jia, S., Mao, J., Yan, F., Wang, X., and Shao, M.: Synergistic effects of  
559 biogenic volatile organic compounds and soil nitric oxide emissions on summertime ozone formation in  
560 China, *Science of The Total Environment*, 828, 154218, 2022.

561 Clappier, A., Belis, C. A., Pernigotti, D., and Thunis, P.: Source apportionment and sensitivity analysis:  
562 two methodologies with two different purposes, *Geoscientific Model Development*, 10, 4245-4256,  
563 2017.

564 Council, S.: The 14th Five-Year Plan for National Economic and Social Development of the People's  
565 Republic of China and the Outline of Long-Term Objectives for 2035, 2021.

566 Diao, B., Ding, L., Su, P., and Cheng, J.: The spatial-temporal characteristics and influential factors of  
567 NO<sub>x</sub> emissions in China: A spatial econometric analysis, *International journal of environmental*  
568 *research and Public Health*, 15, 1405, 2018.

569 Ding, D., Xing, J., Wang, S., Dong, Z., Zhang, F., Liu, S., and Hao, J.: Optimization of a NO<sub>x</sub> and  
570 VOC cooperative control strategy based on clean air benefits, *Environmental Science & Technology*,  
571 56, 739-749, 2021.

572 Ding, L., Liu, C., Chen, K., Huang, Y., and Diao, B.: Atmospheric pollution reduction effect and  
573 regional predicament: An empirical analysis based on the Chinese provincial NO<sub>x</sub> emissions, *Journal*  
574 *of environmental management*, 196, 178-187, 2017.

575 Drury, C. F., Reynolds, W. D., Yang, X., McLaughlin, N. B., Calder, W., and Phillips, L. A.: Diverse  
576 rotations impact microbial processes, seasonality and overall nitrous oxide emissions from soils, *Soil*  
577 *Science Society of America Journal*, 85, 1448-1464, 2021.

578 Du, L., Zhao, H., Tang, H., Jiang, P., and Ma, W.: Analysis of the synergistic effects of air pollutant  
579 emission reduction and carbon emissions at coal - fired power plants in China, *Environmental Progress*  
580 *& Sustainable Energy*, 40, e13630, 2021.

581 Dunker, A. M., Koo, B., and Yarwood, G.: Source apportionment of the anthropogenic increment to  
582 ozone, formaldehyde, and nitrogen dioxide by the path-integral method in a 3D model, *Environmental*  
583 *science & technology*, 49, 6751-6759, 2015.

584 The volatile organic compound management attack program in 2020 (in Chinese): (available  
585 at:[www.mee.gov.cn/xxgk/xxgk03/202006/t20200624\\_785827.html](http://www.mee.gov.cn/xxgk/xxgk03/202006/t20200624_785827.html)), last  
586 Feng, Z., De Marco, A., Anav, A., Gualtieri, M., Sicard, P., Tian, H., Fornasier, F., Tao, F., Guo, A., and  
587 Paoletti, E.: Economic losses due to ozone impacts on human health, forest productivity and crop yield  
588 across China, *Environment international*, 131, 104966, 2019.

589 Galbally, I. E., Kirstine, W. V., Meyer, C., and Wang, Y. P.: Soil-atmosphere trace gas exchange in  
590 semiarid and arid zones, *Journal of Environmental Quality*, 37, 599-607, 2008.

591 Guo, L., Chen, J., Luo, D., Liu, S., Lee, H. J., Motallebi, N., Fong, A., Deng, J., Rasool, Q. Z., and  
592 Avise, J. C.: Assessment of nitrogen oxide emissions and San Joaquin Valley PM<sub>2.5</sub> impacts from soils  
593 in California, *Journal of Geophysical Research: Atmospheres*, 125, e2020JD033304, 2020.

594 Heffer, P. and Prud'homme, M.: Global nitrogen fertilizer demand and supply: Trend, current level and  
595 outlook, International Nitrogen Initiative Conference. Melbourne, Australia,

596 Huang, K., Su, C., Liu, D., Duan, Y., Kang, R., Yu, H., Liu, Y., Li, X., Gurmesa, G. A., and Quan, Z.: A  
597 strong temperature dependence of soil nitric oxide emission from a temperate forest in Northeast  
598 China, *Agricultural and Forest Meteorology*, 323, 109035, 2022a.

599 Huang, L., Kimura, Y., and Allen, D. T.: Assessing the impact of episodic flare emissions on ozone  
600 formation in the Houston-Galveston-Brazoria area of Texas, *Science of The Total Environment*, 828,  
601 154276, 2022b.

602 Huang, L., Wang, Q., Wang, Y., Emery, C., Zhu, A., Zhu, Y., Yin, S., Yarwood, G., Zhang, K., and Li,  
603 L.: Simulation of secondary organic aerosol over the Yangtze River Delta region: The impacts from the  
604 emissions of intermediate volatility organic compounds and the SOA modeling framework,  
605 *Atmospheric Environment*, 246, 118079, 2021.

606 Huber, D. E., Steiner, A. L., and Kort, E. A.: Sensitivity of Modeled Soil NO<sub>x</sub> Emissions to Soil  
607 Moisture, *Journal of Geophysical Research: Atmospheres*, 128, e2022JD037611, 2023.

608 Hudman, R. C., Moore, N. E., Mebust, A. K., Martin, R. V., Russell, A. R., Valin, L. C., and Cohen, R.  
609 C.: Steps towards a mechanistic model of global soil nitric oxide emissions: implementation and space  
610 based-constraints, *Atmospheric Chemistry and Physics*, 12, 7779-7795, 10.5194/acp-12-7779-2012,  
611 2012.

612 Jiang, Y., Wang, S., Xing, J., Zhao, B., Li, S., Chang, X., Zhang, S., and Dong, Z.: Ambient fine  
613 particulate matter and ozone pollution in China: synergy in anthropogenic emissions and atmospheric  
614 processes, *Environmental Research Letters*, 17, 123001, 2022.

615 Kleinman, L., Lee, Y. N., Springston, S. R., Nunnermacker, L., Zhou, X., Brown, R., Hallock, K.,  
616 Klotz, P., Leahy, D., and Lee, J. H.: Ozone formation at a rural site in the southeastern United States,  
617 *Journal of Geophysical Research: Atmospheres*, 99, 3469-3482, 1994.

618 Koo, B., Wilson, G. M., Morris, R. E., Dunker, A. M., and Yarwood, G.: Comparison of source  
619 apportionment and sensitivity analysis in a particulate matter air quality model, *Environmental science  
620 & technology*, 43, 6669-6675, 2009.

621 Lin, Y., Jiang, F., Zhao, J., Zhu, G., He, X., Ma, X., Li, S., Sabel, C. E., and Wang, H.: Impacts of O<sub>3</sub>  
622 on premature mortality and crop yield loss across China, *Atmospheric Environment*, 194, 41-47, 2018.

623 Liu, H. Z., Qingqing Liu: Distribution of Fertilizer Application and Its Environmental Risk in Different  
624 Provinces of China, *Chemical Management*, 174-174, 2016.

625 Liu, P., Song, H., Wang, T., Wang, F., Li, X., Miao, C., and Zhao, H.: Effects of meteorological  
626 conditions and anthropogenic precursors on ground-level ozone concentrations in Chinese cities,  
627 *Environmental Pollution*, 262, 114366, 2020.

628 Liu, X., Zhang, Y., Han, W., Tang, A., Shen, J., Cui, Z., Vitousek, P., Erisman, J. W., Goulding, K., and  
629 Christie, P.: Enhanced nitrogen deposition over China, *Nature*, 494, 459-462, 2013.

630 Lü, C. and Tian, H.: Spatial and temporal patterns of nitrogen deposition in China: synthesis of  
631 observational data, *Journal of Geophysical Research: Atmospheres*, 112, 2007.

632 Lu, X., Zhang, L., Wang, X., Gao, M., Li, K., Zhang, Y., Yue, X., and Zhang, Y.: Rapid increases in  
633 warm-season surface ozone and resulting health impact in China since 2013, *Environmental Science &  
634 Technology Letters*, 7, 240-247, 2020.

635 Lu, X., Ye, X., Zhou, M., Zhao, Y., Weng, H., Kong, H., Li, K., Gao, M., Zheng, B., and Lin, J.: The  
636 underappreciated role of agricultural soil nitrogen oxide emissions in ozone pollution regulation in  
637 North China, *Nature communications*, 12, 5021, 2021.

638 Maji, K. J.: Substantial changes in PM<sub>2.5</sub> pollution and corresponding premature deaths across China  
639 during 2015–2019: A model prospective, *Science of the Total Environment*, 729, 138838, 2020.

640 Malley, C. S., Henze, D. K., Kuylenstierna, J. C., Vallack, H. W., Davila, Y., Anenberg, S. C., Turner,  
641 M. C., and Ashmore, M. R.: Updated global estimates of respiratory mortality in adults  $\geq 30$  years of  
642 age attributable to long-term ozone exposure, *Environmental health perspectives*, 125, 087021, 2017.

643 Mao, J., Wang, L., Lu, C., Liu, J., Li, M., Tang, G., Ji, D., Zhang, N., and Wang, Y.: Meteorological  
644 mechanism for a large-scale persistent severe ozone pollution event over eastern China in 2017, *Journal*  
645 *of Environmental Sciences*, 92, 187-199, 2020.

646 Montes, C. M., Demler, H. J., Li, S., Martin, D. G., and Ainsworth, E. A.: Approaches to investigate  
647 crop responses to ozone pollution: from O<sub>3</sub> - FACE to satellite - enabled modeling, *The Plant Journal*,  
648 109, 432-446, 2022.

649 Mukherjee, A., Yadav, D. S., Agrawal, S. B., and Agrawal, M.: Ozone a persistent challenge to food  
650 security in India: current status and policy implications, *Current Opinion in Environmental Science &*  
651 *Health*, 19, 100220, 2021.

652 Oikawa, P., Ge, C., Wang, J., Eberwein, J., Liang, L., Allsman, L., Grantz, D., and Jenerette, G.:  
653 Unusually high soil nitrogen oxide emissions influence air quality in a high-temperature agricultural  
654 region, *Nature communications*, 6, 8753, 2015.

655 Park, J., Shin, M., Lee, J., and Lee, J.: Estimating the effectiveness of vehicle emission regulations for  
656 reducing NO<sub>x</sub> from light-duty vehicles in Korea using on-road measurements, *Science of The Total*  
657 *Environment*, 767, 144250, 2021.

658 Potter, P., Ramankutty, N., Bennett, E. M., and Donner, S. D.: Characterizing the spatial patterns of  
659 global fertilizer application and manure production, *Earth interactions*, 14, 1-22, 2010.

660 Ramboll: User's Guide: Comprehensive Air quality Model with extensions, Version 7.1., 2021.

661 Rasool, Q. Z., Zhang, R., Lash, B., Cohan, D. S., Cooter, E. J., Bash, J. O., and Lamsal, L. N.:  
662 Enhanced representation of soil NO emissions in the Community Multiscale Air Quality (CMAQ)  
663 model version 5.0. 2, *Geoscientific Model Development*, 9, 3177-3197, 2016.

664 Romer, P. S., Duffey, K. C., Wooldridge, P. J., Edgerton, E., Baumann, K., Feiner, P. A., Miller, D. O.,  
665 Brune, W. H., Koss, A. R., and De Gouw, J. A.: Effects of temperature-dependent NO<sub>x</sub> emissions on  
666 continental ozone production, *Atmospheric Chemistry and Physics*, 18, 2601-2614, 2018.

667 Seinfeld, J. H. and Pandis, S. N.: *Atmospheric chemistry and physics: from air pollution to climate*  
668 *change*, John Wiley & Sons 2016.

669 Sha, T., Ma, X., Zhang, H., Janecek, N., Wang, Y., Wang, Y., Castro García, L., Jenerette, G. D., and  
670 Wang, J.: Impacts of Soil NO<sub>x</sub> Emission on O<sub>3</sub> Air Quality in Rural California, *Environmental science*  
671 *& technology*, 55, 7113-7122, 2021.

672 Shen, L., Liu, J., Zhao, T., Xu, X., Han, H., Wang, H., and Shu, Z.: Atmospheric transport drives  
673 regional interactions of ozone pollution in China, *Science of The Total Environment*, 830, 154634,  
674 2022.

675 Shen, Y., Xiao, Z., Wang, Y., Xiao, W., Yao, L., and Zhou, C.: Impacts of agricultural soil NO<sub>x</sub>  
676 emissions on O<sub>3</sub> over Mainland China, *Journal of Geophysical Research: Atmospheres*,  
677 e2022JD037986, 2023.

678 Sillman, S., Logan, J. A., and Wofsy, S. C.: The sensitivity of ozone to nitrogen oxides and  
679 hydrocarbons in regional ozone episodes, *Journal of Geophysical Research: Atmospheres*, 95, 1837-  
680 1851, 1990.

681 Skiba, U., Medinets, S., Cardenas, L. M., Carnell, E. J., Hutchings, N., and Amon, B.: Assessing the  
682 contribution of soil NO<sub>x</sub> emissions to European atmospheric pollution, *Environmental Research*  
683 *Letters*, 16, 025009, 2021.

684 Sun, W., Shao, M., Granier, C., Liu, Y., Ye, C., and Zheng, J.: Long - term trends of Anthropogenic  
685 SO<sub>2</sub>, NO<sub>x</sub>, CO, and NMVOCs emissions in China, *Earth's Future*, 6, 1112-1133, 2018.

686 Sun, Y., Yin, H., Lu, X., Notholt, J., Palm, M., Liu, C., Tian, Y., and Zheng, B.: The drivers and health  
687 risks of unexpected surface ozone enhancements over the Sichuan Basin, China, in 2020, *Atmospheric*  
688 *Chemistry and Physics*, 21, 18589-18608, 2021.

689 Thunis, P., Clappier, A., Tarrasón, L., Cuvelier, C., Monteiro, A., Pisoni, E., Wesseling, J., Belis, C.,  
690 Pirovano, G., and Janssen, S.: Source apportionment to support air quality planning: Strengths and  
691 weaknesses of existing approaches, *Environment International*, 130, 104825, 2019.

692 Vinken, G., Boersma, K., Maasakkers, J., Adon, M., and Martin, R.: Worldwide biogenic soil NO<sub>x</sub>  
693 emissions inferred from OMI NO<sub>2</sub> observations, *Atmospheric Chemistry and Physics*, 14, 10363-  
694 10381, 2014.

695 Wang, J., Wang, D., Ge, B., Lin, W., Ji, D., Pan, X., Li, J., and Wang, Z.: Increase in daytime ozone  
696 exposure due to nighttime accumulation in a typical city in eastern China during 2014–2020,  
697 *Atmospheric Pollution Research*, 13, 101387, 2022a.

698 Wang, P., Wang, T., and Ying, Q.: Regional source apportionment of summertime ozone and its  
699 precursors in the megacities of Beijing and Shanghai using a source-oriented chemical transport model,  
700 *Atmospheric Environment*, 224, 117337, 2020.

701 Wang, Q. g., Han, Z., Wang, T., and Zhang, R.: Impacts of biogenic emissions of VOC and NO<sub>x</sub> on  
702 tropospheric ozone during summertime in eastern China, *Science of the total environment*, 395, 41-49,  
703 2008.

704 Wang, R., Bei, N., Wu, J., Li, X., Liu, S., Yu, J., Jiang, Q., Tie, X., and Li, G.: Cropland nitrogen  
705 dioxide emissions and effects on the ozone pollution in the North China plain, *Environ Pollut*, 294,  
706 118617, 10.1016/j.envpol.2021.118617, 2022b.

707 Wang, Y., Ge, C., Garcia, L. C., Jenerette, G. D., Oikawa, P. Y., and Wang, J.: Improved modelling of  
708 soil NO<sub>x</sub> emissions in a high temperature agricultural region: role of background emissions on NO<sub>2</sub>  
709 trend over the US, *Environmental research letters*, 16, 084061, 2021.

710 Xiao, Q., Geng, G., Liang, F., Wang, X., Lv, Z., Lei, Y., Huang, X., Zhang, Q., Liu, Y., and He, K.:  
711 Changes in spatial patterns of PM<sub>2.5</sub> pollution in China 2000–2018: Impact of clean air policies,  
712 *Environment international*, 141, 105776, 2020.

713 Xue, C., Ye, C., Liu, P., Zhang, C., Su, H., Bao, F., Cheng, Y., Catoire, V., Ma, Z., and Zhao, X.: Strong  
714 HONO Emissions from Fertilized Soil in the North China Plain 4 Driven by Nitrification and Water  
715 Evaporation, 2022.

716 Yan, X., Ohara, T., and Akimoto, H.: Statistical modeling of global soil NO<sub>x</sub> emissions, *Global*  
717 *Biogeochemical Cycles*, 19, 2005.

718 Yang, X., Wu, K., Lu, Y., Wang, S., Qiao, Y., Zhang, X., Wang, Y., Wang, H., Liu, Z., and Liu, Y.:  
719 Origin of regional springtime ozone episodes in the Sichuan Basin, China: role of synoptic forcing and  
720 regional transport, *Environmental Pollution*, 278, 116845, 2021.

721 Yarwood, G., Morris, R., Yocke, M., Hogo, H., and Chico, T.: Development of a methodology for  
722 source apportionment of ozone concentration estimates from a photochemical grid model, AIR &  
723 WASTE MANAGEMENT ASSOCIATION, PITTSBURGH, PA 15222(USA).[np]. 1996.

724 Yarwood, G., Jung, J., Whitten, G. Z., Heo, G., Mellberg, J., and Estes, M.: Updates to the Carbon  
725 Bond mechanism for version 6 (CB6), 9th Annual CMAS Conference, Chapel Hill, NC, 11-13,

726 Yienger, J. and Levy, H.: Empirical model of global soil - biogenic NO<sub>x</sub> emissions, Journal of  
727 Geophysical Research: Atmospheres, 100, 11447-11464, 1995.

728 Yin, H., Lu, X., Sun, Y., Li, K., Gao, M., Zheng, B., and Liu, C.: Unprecedented decline in summertime  
729 surface ozone over eastern China in 2020 comparably attributable to anthropogenic emission reductions  
730 and meteorology, Environmental Research Letters, 16, 124069, 2021.

731 Zhai, S., Jacob, D. J., Wang, X., Shen, L., Li, K., Zhang, Y., Gui, K., Zhao, T., and Liao, H.: Fine  
732 particulate matter (PM<sub>2.5</sub>) trends in China, 2013–2018: separating contributions from anthropogenic  
733 emissions and meteorology, Atmospheric Chemistry and Physics, 19, 11031-11041, 2019.

734 Zheng, B., Zhang, Q., Geng, G., Chen, C., Shi, Q., Cui, M., Lei, Y., and He, K.: Changes in China's  
735 anthropogenic emissions and air quality during the COVID-19 pandemic in 2020, Earth System  
736 Science Data, 13, 2895-2907, 2021.

737 Zhu, Q., Place, B., Pfannerstill, E. Y., Tong, S., Zhang, H., Wang, J., Nussbaumer, C. M., Wooldridge,  
738 P., Schulze, B. C., and Arata, C.: Direct observations of NO<sub>x</sub> emissions over the San Joaquin Valley  
739 using airborne flux measurements during RECAP-CA 2021 field campaign, Atmospheric chemistry and  
740 physics, 23, 9669-9683, 2023.

741